This version is a preprint published at: Mateus, R., et al. “Helium Load on W-O Coatings Grown by Pulsed Laser Deposition.” *Surface and Coatings Technology*, vol. 355, Dec. 2018, pp. 215–21. *DOI.org (Crossref)*, doi:10.1016/j.surfcoat.2018.02.089.

Helium load on W-O coatings grown by pulsed laser deposition

R. Mateus[1,*], D. Dellasega[2,3], M. Passoni[2,3], Z. Siketić[4],
I. Bogdanović Radović[4], A. Hakola[5], E. Alves[1]

[1]*Instituto de Plasmas e Fusão Nuclear, Instituto Superior Técnico, Universidade de Lisboa, Av. Rovisco Pais, 1049-001 Lisboa, Portugal*

[2]*Dipartimento di Energia, Politecnico di Milano, via Ponzio 34/3, 20133 Milano, Italy*

[3]*IFP, CNR, via R. Cozzi 53, Milano 20125, Italy*

[4]*Ruder Bošković Institute, P.O. Box 180, 10002 Zagreb, Croatia*

[5]*VTT Technical Research Centre of Finland Ltd., Finland*

*corresponding author: rmateus@ipfn.ist.utl.pt

Abstract

W-O deposits with complex morphologies and significant He contents will growth on the surface of plasma facing components exposed to He discharges. To mimic the re/co-deposition process, W-O-He coatings were produced by implanting He^+ ions on W films grown by pulsed laser deposition (PLD). The use of appropriate PLD experimental parameters such as Ar or He background atmospheres induces the deposition of porous or amorphous-like W-O structures, respectively. After multiple ion implantation stages using 150 keV, 100 keV and 50 keV incident He^+ ion beams with a total fluence of 5 x 10^{17} ion/cm^2, significant amounts of He were identified in porous coatings by Rutherford backscattering (RBS). Time-of-flight elastic recoil detection (TOF-ERDA) measurements showed that most of the implanted He was already released from the porous coatings five month after implantation while for the case of amorphous ones the He content remains significant at deeper layers and smoothly decrease towards the surface, as result of a different morphology and nanostructure. The proposed method involving PLD and ion implantation seems adequate to produce W-O-He reference samples for fusion investigations.

Keywords: PLD, W coatings, ion implantation, helium load

1. Introduction

During the operation of fusion devices the plasma will strongly interact with plasma facing components (PFC) leading to the erosion of the exposed surfaces, re-deposition of eroded material and environment impurities as oxygen (O), and trapping of fuel as well as isotopic products (He-4) of the D-T reaction [1]. Tungsten (W) is the chosen material for the divertor of ITER [1] and the use of full W PFC walls and divertors is under investigation in different plasma devices [2,3]. Experimental results revealed that the grown deposits may present distinct nano/ microstructures and compositions with various impurities. This is the case of compact and amorphous W-O layers covering optical mirrors located at the first wall and divertor of the ASDEX Upgrade tokamak [2], and of porous W-O deposits found on the outer divertor strike point tiles of the same device [3]. The effects caused by deuterium and helium plasma exposure may be related to the different W-O structures. There is therefore need to determine the outcomes arising from the modifications in dedicated experiments to predict the properties and lifetimes of the irradiated PFCs. To this purpose, W-O coatings loaded with deuterium or helium (He) and resembling possible re-deposited layers on PFCs in W-based fusion devices are being produced under the EUROfusion consortium [4-6]. The present work reports part of the activities aiming the production of suitable W-O-He coatings involving two very different W morphologies: porous W with an open nanocrystalline structure and amorphous-like W with a compact morphology and poor crystallinity. Aim of the study is the investigation, using ion beam analysis, of He loading and release dynamics in the different W-O nanostructured layers also after long time storage.

2. Experimental procedure

Pulsed Laser Deposition (PLD) technique has been exploited to produce appropriate coatings for the research using a pure metallic W target as W source and a proper background pressure of argon (Ar) or He. The role of different PLD parameters in the deposition procedure, such as the wavelength of the laser beam used to ablate the W source (532 nm in this case), the laser fluence per pulse (close to 15 J/cm^2), the target-to-substrate distance (7 cm) or the pressure and composition of the used background gas are detailed elsewhere [4,5]. PLD parameters are properly tailored to produce porous W (p-W) and amorphous-like W (a-W) deposits enriched with O that mimic re-deposited microstructures observed in tokamaks [2,3]. The adhesion of the W-O layers on the stainless steel substrates is reinforced by using a pure and thin 150 nm crystalline W interface deposited initially in vacuum (10^{-3} Pa). In the present experiment, p-W coatings were prepared by using a 50 Pa Ar atmosphere, promoting a porous morphology with enhanced O contents [4,5]. For the present a-W coatings, a 70 Pa atmosphere of He, the same PLD geometry and similar laser pulses to ablate the W target were used. Table 1 resumes some of the relevant parameters used to growth both p-W and a-W coatings and crystalline W interfaces.

A Zeiss Supra 40 field emission scanning electron microscope assisted with an X-ray detector was used to characterize surface morphologies by scanning electron microscopy (SEM) and quantify the elemental W and O contents by energy dispersion X-ray spectroscopy (EDS). X-ray diffraction measurements were performed with a Panalytical X'Pert PRO X-ray diffractometer in the θ-2θ configuration using a copper (Cu) X-ray source for phase identification. A 210 kV high flux ion implanter was used to irradiate simultaneously and at room temperature all the porous and compact coatings performing multiple implantation stages with normal incidence of $^{4}He^{+}$ ion beams with energies of 150 keV, 100 keV and 50 keV, current densities of 4.3 μm/cm^2 and a total fluence of 5 x 10^{17} at./cm^2, being the depth ranges of the ions within the materials evaluated by the SRIM code [7].

The as-deposited and implanted samples were analysed with ion beam techniques such as elastic backscattering (EBS) and Rutherford backscattering spectroscopies (RBS) making use of 1500 keV H^{+} and of 2000 keV He^{+} ion beams, respectively, with the purpose to directly evaluate the thickness and the W and O elemental depth profiles, being the elemental quantification performed with the NDF code [8]. Also He retained amounts could be evaluated indirectly by RBS from the decrease of the backscattering yields of heavy W in the implanted samples. Time-of-flight elastic recoil detection (TOF-ERDA) experiments using 23 MeV $^{127}I^{6+}$ ion beams at a glancing angle of 20° were also performed to evaluate the release of He from the surfaces and to quantify the presence of a larger number of elements. The analysis of the TOF-ERDA spectra was done using the Potku [9] and CORTEO [10] codes.

3. Results and discussion

3.1 Characterization of p-W and a-W nanostructured coatings

Fig. 1 presents (secondary electron) SEM images of the as-deposited W-O coatings. Two distinct morphologies can be appreciated from the top views of both p-W (a) and a-W films (b) and from the corresponding cross-section images (c) and (d). Fig 1.a evidences the growth of the porous and cauliflower morphology under a pressurized 50 Pa Ar atmosphere. Instead the use of a 70 Pa He atmosphere at the same relevant PLD parameters led to a smooth, compact and featureless growth revealed in Fig. 1.b, while it is difficult to visualize a contrast in the SEM image. The cross-section images confirm the presence of the two distinct nanostructures: the cauliflower morphology on the top view of the porous samples is caused by 100 nm wide tree-like structures that grow perpendicularly respect to the substrate (Fig. 1.c), while the a-W film reveals the same morphology of the top view along its depth (Fig. 1.d). The presence of a crystalline W adhesion layer on the interface between the substrate and the coating is detailed by the magnified view of a cross-section image of a porous sample in Fig. 1.e.

From the XRD diffractograms in Fig. 2 it is possible to characterize the crystallinity of the deposited films. The p-W film exhibits a quite broad reflection centered at 39.8 degrees in the 2θ configuration, evidencing

the growth of a bcc W-based microstructure. Nevertheless, the reported value for the (110) diffraction peak of pure bcc W is about 40.3° [11]. From the Bragg's law, and considering the wavelength of 0.154 nm for the Cu-Kα1 line of the X-ray source, a decrease in the (110) peak close to 0.50 degrees corresponds to an increment of the lattice parameter *a* of the bcc W phase from the reference value of 0.317 nm to about 0.320 nm, and to a lattice expansion $\Delta a/a$ of about 1.2% relative to pure bcc W. The structural swelling is easily justified by addition of O and other impurities in the W unit cell [12,13]. Considering the broadening of the (110) peak, the mean crystallite domain size calculated by using the Scherrer equation is about 7 nm [5,12]. The bcc W like structure in the p-W coatings is also confirmed by the corresponding diffraction peaks detected with lower intensities for planes (200), (112) and (220). On the other side, the diffractogram of a-W shows only a wide and broad band typically centered at the diffraction peak for plane (110) of bcc W. Therefore, the mean crystalline size of the grains in this case is very low, which is the signature for amorphous materials [5,12]. These data show that the porous samples exhibit higher crystallinity respect to the amorphous ones. This may be related to the formation of crystalline nanoparticles during the ablation process due to the interaction with the Ar atmosphere.

The O content, as quantified by EDS in the surface of the p-W films was about 55 at.% [4]. Instead, thanks to its compact morphology, a-W films showed O contents close to 16 at.% [5]. The use of an Ar background atmosphere results in a significant decrease of the kinetic energy of the ablated W atoms impinging on the substrate due to the scattering imposed by the Ar atoms, thus leading to the growth of non-compact but porous structures. Possibly, the high surface-to-volume ratio of these microstructures induces the spontaneous oxidation of the coatings during exposition to ambient air after deposition [4]. In opposition to Ar atmospheres, He has been chosen as the background gas for the formation of a-W coatings because it is the noble gas with the smallest atomic mass and consequently with the lowest thermalizing effect on the ablated atoms. An earlier investigation has shown a structural transition from a crystalline to an amorphous-like growth in the deposits at about 30 Pa by varying the He background pressure in the range from 10^{-3} Pa to 200 Pa [5]. Ranging background pressure, the deposits appear to be formed by even smaller grains, with a corresponding decrease in films density and rise of bcc W lattice parameters. Also the O content may rise quickly from 5% at. to 20 at.%. within a slight pressure change from 40 Pa to 50 Pa. A larger retention of O may be related to the formation of new kinds of defects and energetic traps in the films. Nevertheless, the final O content (15%-20%) is always lower compared to the case of porous deposits (~50%) [5].

3.2 Multiple implantation stages of helium

Earlier implantation experiments with energetic He ions evidenced drastic changes to the surface morphology of polycrystalline W maintained in the 500-900 ºC temperature range when the He fluence exceeded 1 x 10^{18} ion/cm^2, promoting the release of He through channels in the nanoscale created by the

coalescence and movement of He bubbles through the implantation zone [14]. The present irradiation campaign was performed with a total He^+ fluence of 5 x 10^{17} ion/cm^2 keeping the samples at room temperature to avoid major morphological changes that could enhance the degassing of He. Moreover, the final depth ranges were spread out and diluted through the implantation zone by using three different implantation stages with a sequential decrease in the energy of incident ions. The corresponding ion beam energies and fluences of the first, second and third stages were, respectively, 150 keV and 2 x 10^{17} ion/cm^2, 100 keV and 2 x 10^{17} ion/cm^2 and 50 keV and 1 x 10^{17} ion/cm^2. All the p-W and a-W coatings were implanted simultaneously. Therefore, lower energy losses imposed to the incident ions and higher ion ranges are predicted within the p-W coatings, while they present matrixes with lower average Z-values [7,15]. Depth ranges and path length distribution of implanted He were calculated by the SRIM code considering materials with very distinct O contents [7]. The stopping power imposed by W-O matrixes to the incident ions is quantified with a linear combination of the stopping powers calculated for the individual elements with the Bragg's rule, giving rise to very accurate results for the case of heavy elements as O and W [7], that could be present in different W:O ratios along the depth range of the impinging ions. Due to the energy spread of ions in matter, not all the ions implanted with an unique energy take the same depth, and by calculating the average projected range, Rp, the corresponding standard deviation, ΔRp, and by knowing the specific implanted ion fluence, it is possible to predict the depth profile ranges and maximum concentrations of the implanted species with a Gaussian like profile [7,15]. Nevertheless, the calculations do not take into consideration non-uniform W-O depth profiles, the crystalline structure of the target or the role of grain boundaries and lattice defects [7,15]. Table 2 presents the Rp and ΔRp depth ranges calculated for two distinct W:O compositions: pure W and the W:O (37:62) stoichiometry of as-deposited p-W coatings as it was quantified by RBS (see in this section). The total depth profile of He is obviously wider for the porous coatings (with a higher O content) and considering the corresponding depth ranges and ion fluences for the three irradiation stages, a final depth profiles of implanted ions in the porous samples is obtained (see Fig. 3), pointing before the irradiation campaign that the impinging ions will not reach the SS substrate or the W interface neither in porous and, as obviously, nor in amorphous-like coatings. For the present case of multiple implantation stages in p-W samples maximum He contents of about 15 at.% were predicted. Outcomes arising from structural defects will lead to higher retentions of He close to the surface and to lower He depth ranges.

3.3 Helium load and release dynamics on p-W and a-W coatings

Composition of p-W and a-W coatings has been checked as deposited (as-deposited), right after He implantation (as-implanted) and five months after implantation (aged). As-deposited films have been characterized by SEM, EDS, EBS, RBS and TOF-ERDA, as-implanted films have been analysed by EBS

and RBS and aged films have been characterized by EBS, RBS and TOF-ERDA. With the purpose to confirm the origin of retained He, additional TOF-ERDA measurements had been carried out to a new set of p-W and a-W films deposited by PLD at the same experimental parameters.

Fig. 4.a shows the EBS spectra collected from the porous coatings before and after implantation, where the vertical arrows indicate the energies relative to the presence of W and O at the surface layer. From the elastic scattering of incident protons by ^{16}O, $^{16}O(p,p)^{16}O$, significant amounts of O on p-W are quantified. The same behaviour is also visible from the decrease of the backscattering yield of heavier W along the coating's depth. An interface region with pure W (identified as the crystalline W adhesion layer in Fig. 1) is located between the p-W film and the SS substrate. In comparison to the incidence of protons, the energy loss of He ions in matter is much higher, since it depends of the square of the incident ion charge [7,15]. Therefore we are highly sensitive to changes in the superficial depth profile of heavy W by RBS (Fig. 4.b), where an expected decrease in the backscattering W yield after the implantation procedure is observed, being the behaviour explained by the addition of the He impurity [16,17]. Therefore and despite the absence of a He yield, a retained depth profile for He may be quantified by RBS [16,17]. The complementary EBS/RBS analyses in the as-deposited p-W coatings points to an O content close to 62.5 at.% and to coating's thickness of about 111.7 x 10^{17} at/cm^2, followed by a pure W interface close to 9.8 x 10^{17} at/cm^2 (~155 nm considering bulk W density). After implantation the coating's thickness decreases to 107.0 x 10^{17} at./cm^2 due to physical sputtering and a maximum He content of 23.0 at.% is evaluated.

In opposition to the case of p-W, any significant change was observed by comparing the elemental depth profiles of both EBS (Fig. 4.c) and RBS spectra (not presented in Fig. 4) collected from a-W coatings, before and after implantation. Due to the compact nature of the coatings, the erosion by physical sputtering did not occur significantly during irradiation. Moreover, and if a low O content exist, EBS is not sensitive to quantify the existing amount. Additional differences in the elemental profiles were explained by changes in the energy resolution of the detector.

Fig. 5 presents analytical results evidencing changes operated in the He, O and W depth profiles of p-W coatings by ion implantation and, as predicted by SRIM simulations, the maximum retained He amount did not occur at the surface, but at deeper depths. Nevertheless, the simulation shows that the He amount is preferentially retained nearby the surface with maximum contents higher than those predicted by SRIM (23 at.% vs. 15 at.%). The result seems to agree with the gathering of He atoms along structural imperfections in the p-W bcc structure [14].

Ar and He are noble gases, thus insoluble in metals and migrate rapidly through metallic lattices. The trapping in lattice defects or a degassing at the surface should be quite fast [14,18] even at room temperature. Due to the grazing geometry of the analysis, TOF-ERDA is really sensitive to the presence of the individual elements nearby the superficial layers. Very recent TOF-ERDA measurements performed in new and as-deposited W-O films revealed superficial elemental contents for both p-W (15 at.% H, 1.9 at.%

C, 2.5 at.% N, 60 at.% O, 20.6 at.% W) and a-W coatings (2.1 at.% H, 0.7 at.% C, 2.0 at.% N, 25 at.% O, 70 at.% W). Higher contents for H, C, N and O in porous surfaces agree with an easier trapping behaviour of environmental contaminants in a porous structure [18]. Moreover, it is interesting to note that although the deposition of p-W and a-W has been performed in Ar or He background atmospheres [4,5,19] neither Ar nor He are retained in the W coatings prior He ions implantation. As example of the analysis, Fig. 6.a presents the coincident map collected from an as-deposited a-W sample obtained with the particle (ERDA) detector and the two time-of-flight (TOF) detectors, where all the elemental yields are well separated (the yield for I relates with the primary beam).

Although a huge He retention in as-implanted p-W coatings has been observed by RBS (maximum of 23 at.%; see also Fig. 4.b), TOF-ERDA maps confirmed that most of the retained He has been released already from aged p-W coatings five months after implantation (data not shown), while a low 3.1 at.%. average He concentration was quantified along a superficial depth close to 17.0 x 10^{17} at/cm^2. The fast degassing is justified in face of a porous structure acting as a path way through the coatings depth [14,18]. The remaining detected elements were H (7.4 at.%), C (4.2 at.%), N (3.0 at.), O (56 at.%) and W (26 at.%). Nevertheless, an equivalent TOF-ERDA map collected from an aged a-W coating (Fig. 4.b) confirmed that a significant amount of He (13.8 at.%) remains within a depth layer of 12.0 x 10^{17} at/cm^2 five month after irradiation, being the remaining elemental composition H (2.3 at.%), C (2.0 at.%), N (1.3 at.%), O (15 at.%) and W (65 at.%). Fig. 7 shows the quantified elemental depth profiles for W, O and He in aged a-W [10]. In particular, it is observed a smooth increase in the retained He amounts at deeper depths, being the result compatible with He release towards the surface, while significant He amounts remain present at deeper depths.

The O contents measured at different research laboratories by EDS, EBS/RBS and TOF-ERDA of the as-deposited p-W (54 at.%, 62 at.% and 60 at.%, respectively) and a-W coatings (16 at.%, not sensitive by RBS, and 25 at.%, respectively) signalise the accuracy of the analyses and the nature of W structures. All the campaig points ion implantation as a promising technique to load He in W films produced by PLD. Obviously, the lifetime of enriched He films will be distinct for p-W and a-W.

4. Summary

W-O coatings were prepared by PLD to mimic W-O-He deposits in tokamaks. The use of an Ar atmosphere as background gas induced the deposition of porous coatings with a W tree-like microstructure (p-W), while amorphous-like deposits (a-W) are produced by using a He gas pressure. He loading was successfully obtained by ion implantation with a sequential implantation stage involving 150 keV, 100 keV and 50 keV He^+ ion beams, showing that the procedure is suitable to produce W-O-He reference coatings for fusion investigations. Film composition has been assessed by EDS, EBS/RBS and TOF-ERDA showing a substantial agreement between the different techniques. RBS is not sensitive to identify smooth changes in

the depth profiles of retained He as in a-W structures. Conversely TOF-EDA has been demonstrated to be a reliable technique for depth ranges of the order of 1200 x 10^{17} at/cm^2.

He retention dynamics is deeply affected by film morphology, nanostructure and composition. The results evidence that a porous morphology allows to retain huge amounts of He but also a fast release takes place, and five months after implantation, most of the He amount has been released from the surfaces. Compact amorphous-like morphology although less rich of He right after implantation compared to p-W morphology can retain higher amounts of He five months after exposure. The result agrees with a smooth degassing of He and with the existence of significant He amounts at deeper depths in compact a-W, as revealed by TOF-ERDA. Additional experiments should be carried out to characterize the He load and optimize the PLD and ion implantation procedures to produce W-O-He standards.

Acknowledgements

This work has been carried out within the framework of the EUROfusion Consortium and has received funding from the Euratom research and training programme 2014-2018 under grant agreement No 633053. The activity was performed in the scope of the WP PFC programme. IST also received financial support from "Fundação para a Ciência e a Tecnologia" through project UID/FIS/50010/2013. The views and opinions expressed herein do not necessarily reflect those of the European Commission.

References

[1] Kleyn A.W., Cardozo N.J.L., Samm U., Phys. Chem. Chem. Phys., 8, 1761-1774 (2006).

[2] A. Litnovsky et al., Nucl. Fusion, 53, 073033 (20133).

[3] M. Rasinski et al., Fusion Eng. Des., 86, 1753–1756 (2011).

[4] Maffini A., Uccello A., Dellasega D., Passoni M., Nucl. Fusion, 56, 086008 (2016).

[5] Dellasega D., Merlo G., Conti C, Bottani C.E., Passoni M., J. Appl. Phys., 112, 084328 (2012).

[6] S. Brezinsek et al., Nucl. Fusion 57 116041 (2017).

[7] Ziegler J.F., Ziegler M.D., Biersack J.P., Nucl. Instrum. Methods Phys. Res. B, 268, 1818-1823 (2010).

[8] N.P. Barradas, C. Jeynes, R.P. Webb, Appl. Phys. Lett., 71, 291-293 (1997).

[9] K. Arstila et al., Nucl. Instrum. Methods Phys. Res. B, 331, 34-41 (2014).

[10] F. Schiettekatte, Nucl. Instrum. Methods Phys. Res. B, 266, 1880-1885 (2008).

[11] A.L. Giorgi, Physica B, 135, 420-422 (1985).

[12] Cullity B.D., Elements of X-ray Diffraction, second ed., Addison-Wesley, Reading, Massachusetts, USA, 1978.

[13] Mateus R., Sequeira M.C., Porosnicu C., Lungu C.P., Hakola A., Alves E., Nucl. Mater. Energy, 12, 462-467 (2017).

[14] Zenobia S.J., Garrison L.M., Kulcinski G.L., J. Nucl. Mater., 425, 83-92 (2012).

[15] Ryssel H. and Ruge I., Ion implantation, Wiley, Chichester, 1986.

[16] Mateus R. et al., J. Nucl. Mater., 442, S251-S255 (2013).

[17] Dias M. et al., J. Nucl. Mater., 442, 69-74 (2013).

[18] Sharafat S. et al., J. Nucl. Mater., 347, 217-243 (2005).

[19] Besozzi E., Dellasega D., Pezzoli A., Conti C., Passoni M., Beghi M.G., Mater. Des., 106, 14-21 (2016).

Table 1

Relevant PLD parameters used to grow p-W, a-W and W adhesion layers.

Parameter	porous W-O	nano W-O	W adhesion layer
backgroud gas	Ar	He	vacuum
gas pressure	50 Pa	70 Pa	10^{-3} Pa
film thickness	1 μm	1 μm	0.15 μm

Table 2
Depth ranges of incident He^+ ions on pure W and on W:O (37:62) simulated by SRIM.

incident beam	pure W		W:O (37:62)	
	Rp (nm)	ΔRp (nm)	Rp (nm)	ΔRp (nm)
150 keV D^+	287	99	556	166
100 keV D^+	207	81	406	139
50 keV D^+	119	54	233	95

Figure Captions

Fig. 1. SEM images of W-O coatings: top views for porous (a) and nanostructured (b) coatings and corresponding cross-section views in (c) and (d); detail of a cross-section view of a porous coating (e).

Fig. 2. XRD diffractograms collected from both p-W and a-W coatings.

Fig. 3. Simulated depth profiles of incident He ions on W:O (37:62) by SRIM

Fig. 4. EBS (a) and RBS spectra (b) of p-W coatings and EBS spectra of nanostructured coatings (c) collected before and after He^{+} implantation.

Fig. 5. W, O and He depth profiles in as-deposited (*) and in as-implanted (**) p-W coatings quantified by EBS/RBS.

Fig. 6. TOF-ERDA overlapped coincidence maps of an as-deposited a-W (a) and of the implanted a-W (b) coating.

Fig.7. W, O and He depth profiles in implanted a-W quantified by TOF-ERDA.

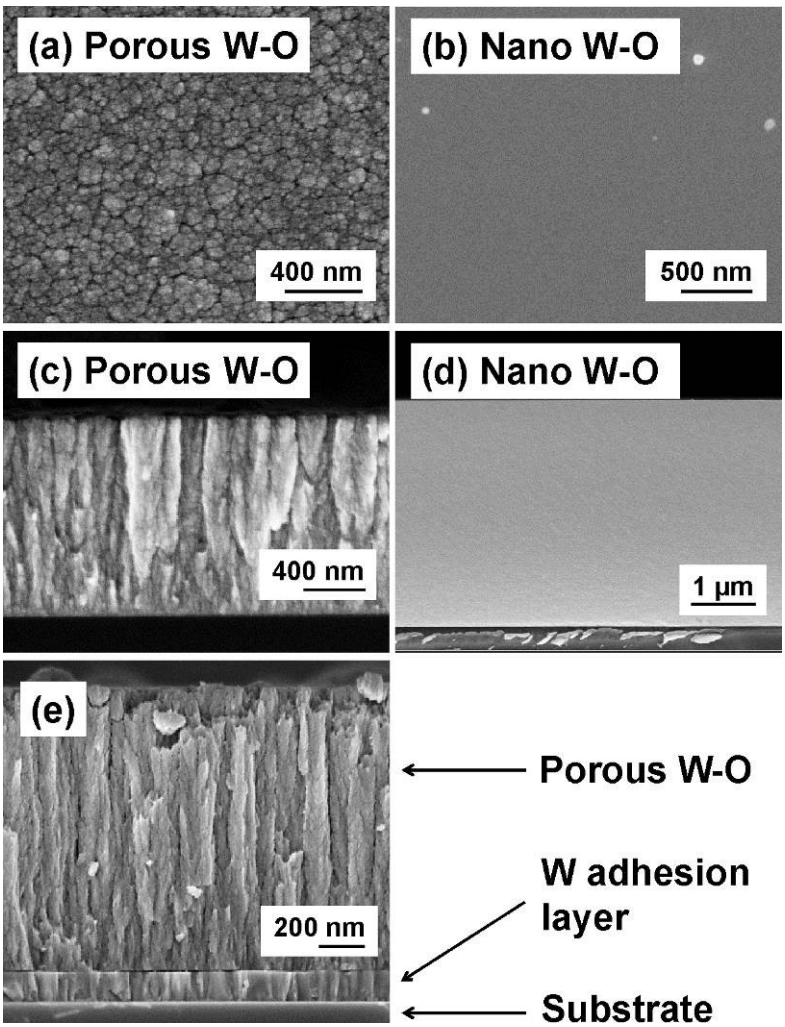
(a) Porous W-O
400 nm
(b) Nano W-O
500 nm
(c) Porous W-O
400 nm
(d) Nano W-O
1 μm
(e)
200 nm
Porous W-O
W adhesion layer
Substrate

Fig. 1

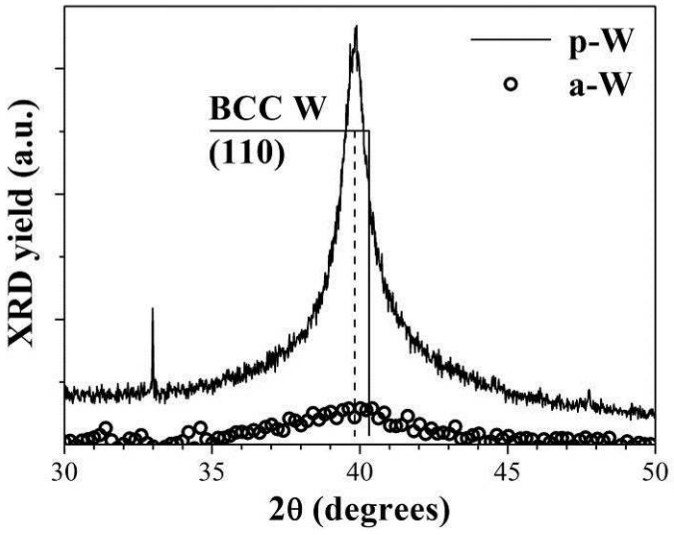
p-W
a-W
BCC W
(110)
XRD yield (a.u.)
30
35
40
45
50
2θ (degrees)

Fig. 2

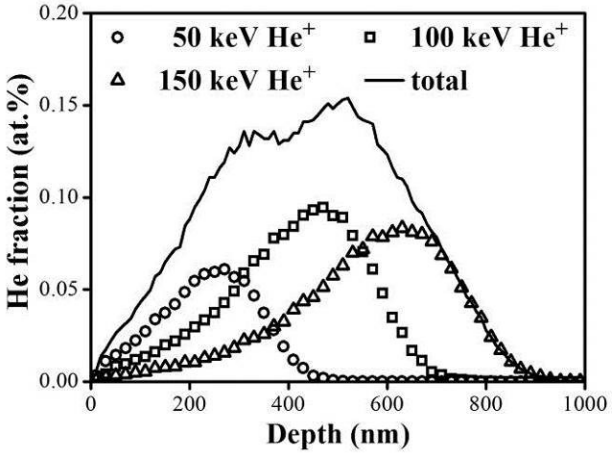
50 keV He+
100 keV He+
150 keV He+
total
He fraction (at.%)
0.20
0.15
0.10
0.05
0.00
0
200
400
600
800
1000
Depth (nm)

Fig. 3

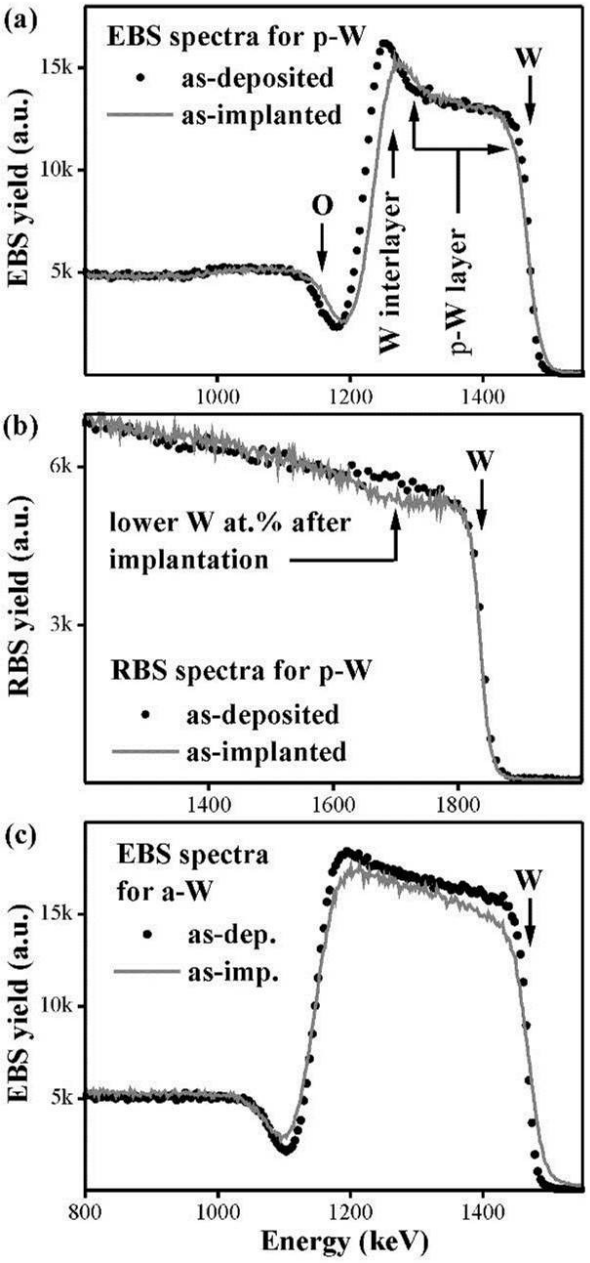
(a)
EBS spectra for p-W
as-deposited
as-implanted
W
O
W interlayer
p-W layer
EBS yield (a.u.)
15k
10k
5k
1000
1200
1400
(b)
W
lower W at.% after implantation
RBS spectra for p-W
as-deposited
as-implanted
RBS yield (a.u.)
6k
3k
1400
1600
1800
(c)
EBS spectra for a-W
as-dep.
as-imp.
W
EBS yield (a.u.)
15k
10k
5k
800
1000
1200
1400
Energy (keV)

Fig. 4

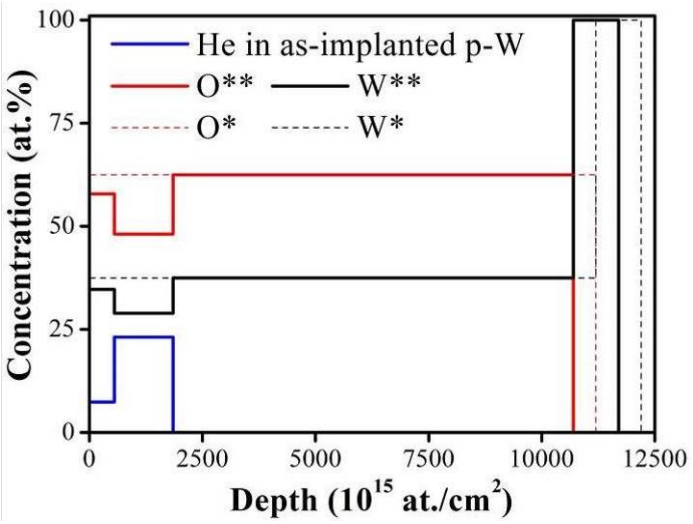
He in as-implanted p-W
O**
W**
O*
W*
Concentration (at.%)
Depth (10^15 at./cm^2)
0
25
50
75
100
0
2500
5000
7500
10000
12500

Fig. 5

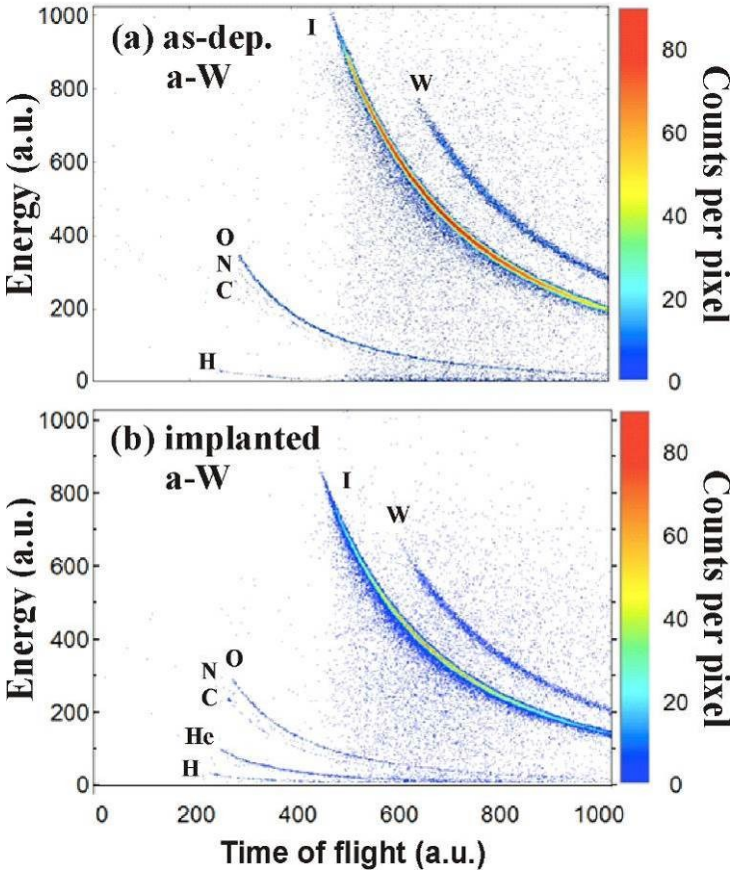
(a) as-dep.
a-W
I
W
O
N
C
H
(b) implanted
a-W
I
W
N
O
C
He
H
Energy (a.u.)
Time of flight (a.u.)
Counts per pixel
0
200
400
600
800
1000
0
20
40
60
80

Fig. 6

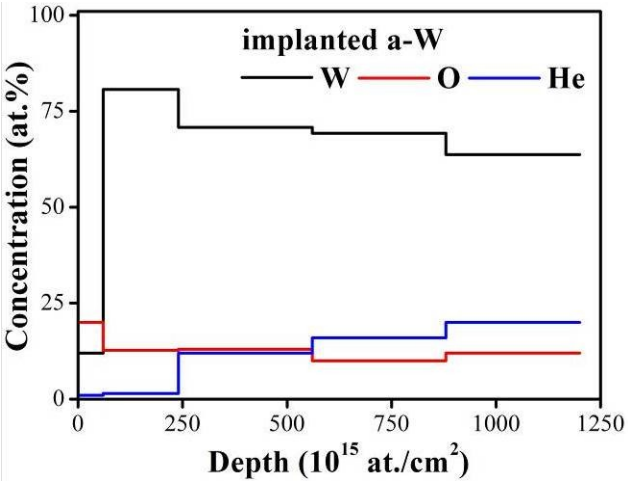
implanted a-W
W
O
He
Concentration (at.%)
100
75
50
25
0
0
250
500
750
1000
1250
Depth (10^{15} at./cm^2)

Fig. 7